

Nano Structured Reduced Graphene Oxide (RGO) Coated TiO₂ as Negative Electrode Additive for Advanced Lead acid Batteries

A Project Report Submitted
as part of the requirements for the degree of

MASTER OF SCIENCE

By

SWATI JINDAL

(Roll No. CY14MSCST11023)

Under the supervision of

Surendra K. Martha



to the
DEPARTMENT OF CHEMISTRY
INDIAN INSTITUTE OF TECHNOLOGY HYDERABAD
INDIA
APRIL, 2016

Declaration

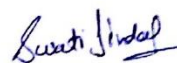
I hereby declare that the matter embodied in this report is the result of investigation carried out by me in the Department of Chemistry, Indian Institute of Technology Hyderabad under the supervision of Dr. Surendra Kumar Martha

In keeping with general practice of reporting scientific observations, due acknowledgement has been made wherever the work described is based on the findings of other investigators.

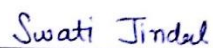


Signature of the Supervisor

Dr. SURENDRA K. MARTHA
Assistant Professor
Department of Chemistry
Indian Institute of Technology Hyderabad



(Signature)



(- Student Name -)



(Roll No)

Approval Sheet

This thesis entitled Nano Structured Reduced Graphene Oxide (RGO) Coated TiO₂ as a Negative Electrode Additive for Advanced Lead acid Batteries by Swati Jindal is approved for the degree of Master of Science.



Dr. M. Deepa M. Deepa (Examiner)
Head & Associate Professor Head of department
Department of Chemistry Department of Chemistry
Indian Institute of Technology Hyderabad Indian Institute of Technology Hyderabad
Kandi-502285, Sangareddy, Telangana, India Kandi-502285, Sangareddy, Telangana, India



Ch. Subrahmanya (Examiner)
Dr. Ch. Subrahmanya
Associate Professor
Department of Chemistry
Indian Institute of Technology Hyderabad
Yeddumailaram, 502 205, A. P., INDIA



Surendra K. Martha (Adviser)
Assistant Professor
Department of Chemistry
Dr. SURENDRA K. MARTHA
Assistant Professor
Department of Chemistry
Indian Institute of Technology Hyderabad

Acknowledgements

Foremost, I would like to express my sincere gratitude to my research supervisor Dr. Surendra Kumar Martha for the continuous support for my M.Sc. study and research, for his patience, motivation, enthusiasm and immense knowledge. His guidance helped me during my research and writing of my thesis. Throughout, my whole M.Sc. he motivated me a lot towards my career. Besides my advisor, I would like to thank the whole faculty of Chemistry department.

My Sincere thanks to the Research Scholar Mr. Naresh Vengapally, who guided me and equally contributed to this work.

I would like to thank my friends: Swati, Saima, Shivangi, Shefali and my class mates for their support.

Last but not the least, I would like to thank my family: my parents Mr. Mahendar Jindal and Mrs. Raj Rani Jindal for giving birth to me at first place and my brother Prashant Jindal for supporting me spiritually throughout my life.

Dedicated to

To my Friends and Family.....

Abstract

Lead-acid batteries (LABs) remains to be the most successful energy storage systems ever developed. Although lead-acid battery designs have been optimized in the past in several different ways, there are still certain challenges facing lead-acid battery designers, such as grid corrosion at the positive electrode, sulfation at both the electrodes, and poor charge acceptance of positive electrode, larger curing and formation time and more significantly low energy density because of high atomic weight of lead. So the current research efforts in electrochemical energy storage are directed towards achieving high energy density with reduced cost and less weight and reduce sulfation. To overcome the issues of sulfation and formation efficiency of the electrodes we propose here reduced graphene oxide (RGO) coated TiO_2 as a negative electrode additive for advanced Lead Acid Batteries (LAB). Addition of 0.5 wt. % of RGO coated TiO_2 in to the negative active mass reduces sulfation, consequently increase battery formation efficiency from 3 cycle to 1 cycle, 10-20% increase in discharge capacity (C-rate performances). The additive also increases the battery life under high rate discharge conditions.

Graphical abstract:

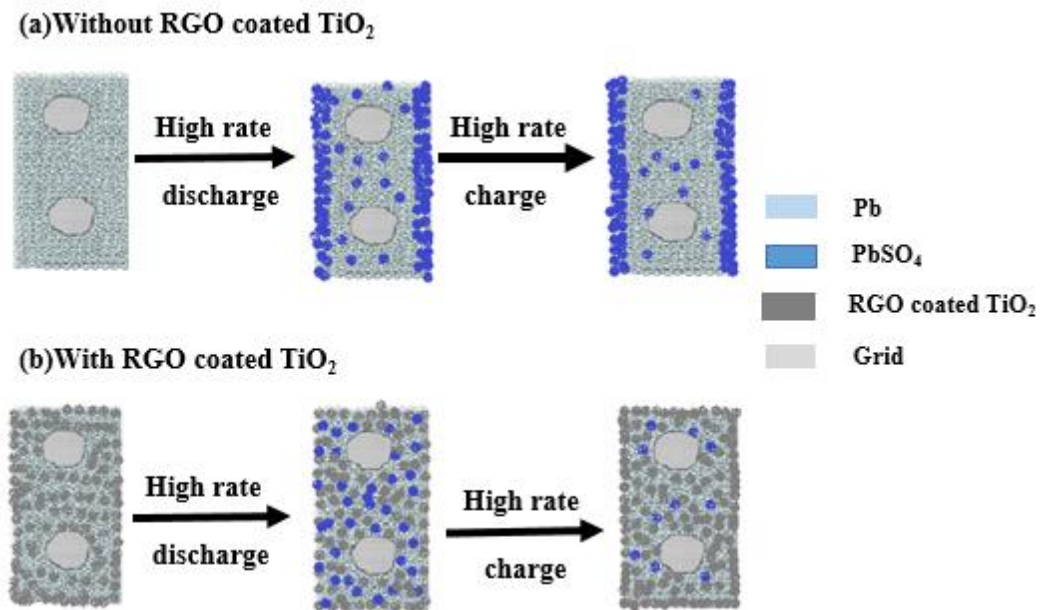


Figure 1: Schematic mechanism of negative electrodes (a) Without RGO coated TiO_2 , (b) With RGO coated TiO_2

Contents

| | |
|-------------------------------------------------------------------------------------------------------------------------------------------------|-------|
| Declaration | 2 |
| Approval Sheet | 3 |
| Acknowledgements | 4 |
| Dedication | 5 |
| Abstract | 6 |
| 1. Introduction to Lead-Acid Battery | |
| 1.1.Introduction | 8 |
| 1.2.Operating Principle | 9-13 |
| References | 14 |
| 2. Nano Structured Reduced Graphene Oxide (RGO) Coated TiO₂ as a Negative Electrode Additive for Advanced Lead acid Batteries | |
| 2.1 Current status | 15-18 |
| 2.2 Experimentals | 19 |
| 2.2.1 Synthesis of Graphene Oxide (GO) by Modified Hummer's Method | 19 |
| 2.2.2 Synthesis of Reduced Graphene Oxide (RGO) coated TiO ₂ by Hydrothermal method | 20 |
| 2.2.3 Fabrication of battery electrodes | 21 |
| 2.2.4 Cell Assembly | 21 |
| 2.2.5 Structural Physical characterizations | 21-22 |
| 2.2.6 Electrochemical measurements | 23 |
| 2.3 Results and Discussions | 23 |
| 2.3.1. X-Ray diffraction | 23-24 |
| 2.3.2 Morphology of GO and RGO-TiO ₂ composite | 24-25 |
| 2.3.3 Morphology of RGO coated TiO ₂ (1:10) by Transmission electron microscopy | 25-26 |
| 2.3.4 Characterization by Raman Spectroscopy | 26-28 |
| 2.3.5 Four Probe Conductivity measurement | 29 |
| 2.3.6 Electrochemical characterizations | 29-34 |
| 2.3.7 Electrochemical Impedance Studies | 35 |
| 2.3.8 Tear-down analysis | 36 |
| 2.3.9 On-going work | 37 |
| Conclusion | 38 |
| References | 39-40 |

Chapter 1

Introduction to Lead-Acid Battery

1.1 Introduction

Raymond Gaston Planté in France developed the lead-acid batteries (LAB) in 1859 and still it is the most widespread battery system ever developed [1-3]. Lead acid battery has tremendous cold-cranking ability, durability, cycle life and low cost, due to which it is tested for the mass market which satisfies the technical requirements for heavy duty applications such as grid, electric vehicles (EVs) and hybrid vehicle (HEVs) applications [4-7]. LABs are famous nowadays due to its safety operation, low cost and greatly availability of materials, easy assembly and a well-known recycling technology, which makes them an attractive candidate for energy storage system [8-10]. The worldwide market is about 50% of all the batteries produced today.

1.2 Operating Principle

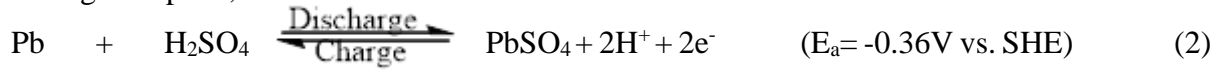
A lead-acid battery comprises several cells connected in series. A lead-acid cell has a negative electrode of spongy lead (negative plate), and a positive electrode of PbO_2 (positive plate) both immersed in an aqueous solution of H_2SO_4 , which not only acts as a conductor of ions but also takes part in the electrode reactions. All lead acid batteries consist of flat lead plates immersed in a pool of 6M H_2SO_4 electrolyte separated by a piece of separator which could be polyethylene, polypropylene or absorptive glass mat (AGM). Every cell has a voltage of around 2.1V when it is in fully charged state [11]. 12.6V battery is produced by connecting the six cells in series. Normally, in lead acid batteries due to water loss electrolyte concentration decreases although low-maintenance types batteries comes with excess of electrolyte so water addition is required. Maintenance free LAB (such as AGM and gelled-electrolyte based) does not need checking of the electrolyte [11-15].

Electrochemistry of the lead acid battery is as follows:

At the positive plate,



At the negative plate,



Accordingly, the net charge-discharge processes in a lead-acid cell are represented by,

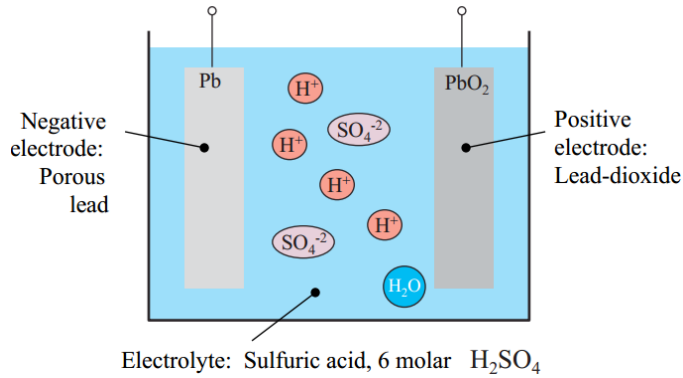
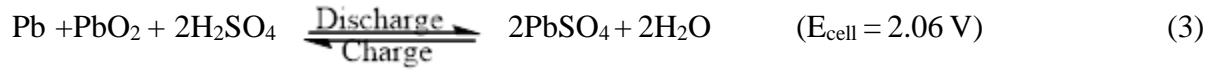


Figure 1.1: Schematic diagram of charge and discharge processes in Lead acid battery

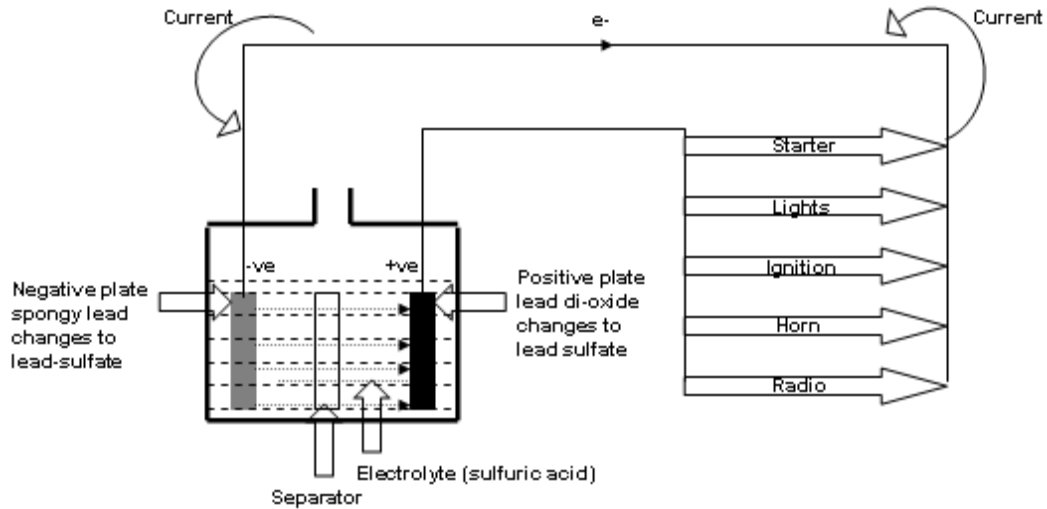
The net cell voltage is approximately 2.06 V which depends on acid concentrations the difference between the cathode voltage 1.7 V and anode voltage 0.36 V [12-15]

During charge and discharge processes, both lead dioxide (PbO_2) on the positive plate and lead (Pb) on the negative plate reacts with 1.26gcm^{-3} of Sulfuric acid (H_2SO_4) to form lead sulphate (PbSO_4) and vice-versa. Both the discharge reactions are accompanied by an increase in volume of the solid phase. The increase in volume for the transformation of PbO_2 to PbSO_4 is 92%, while that of Pb to PbSO_4 is 164% (12-15).

Electrochemical discharge and charge operations for a lead-acid battery are shown in Fig.1.2. During the discharge of a lead-acid cell, electrons flow from its negative plate to the positive plate as shown in Fig.1.2 (a). When the electrons flow from the negative plate to positive plate, they lose their energy. The loss in energy per unit charge is the voltage delivered by the cell. By convention, current flows in the direction opposite to the flow of electrons, and the product of voltage to the current is the power delivered by the cell. An opposite situation occurs during the charging process for the lead-acid cell as shown in Fig. 1.2 (b), where the power is delivered to the cell from an external D.C. source [12-15].

As the cell is discharged, sulfuric acid is consumed and water is formed. Consequently, both the electrolyte composition and density vary from about 40% by weight of H_2SO_4 (1.3 gm/cc) at full charge with an associated open-circuit voltage of 2.15V at 25°C to about 16% by weight of H_2SO_4 (1.10 gm/cc) when fully discharged with an open-circuit voltage of 2.0 V [12-17].

(a) Battery discharging process



(b) Battery charging process

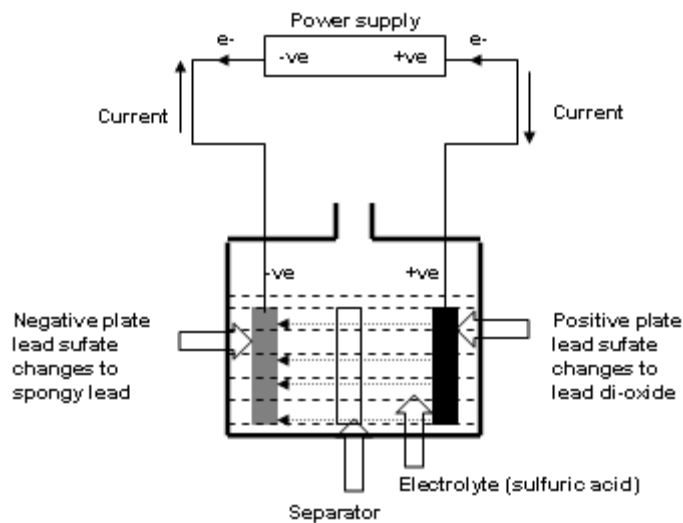


Figure 1.2. Electrochemical (a) discharge and (b) charge operations of a lead-acid battery.

There are secondary reactions occur at the electrode potential within the cell voltage. As the decomposition potential of water is 1.23 V, secondary reactions like hydrogen evolution and oxygen evolution always takes place within the cell according to [16-21]:

Oxygen evolution at the positive electrode:



Hydrogen evolution at the negative electrode:



Overall water decomposition according to



At the potential of positive electrode lead is oxidized to PbO_2 and forms a protective layer according to



In the case of flooded electrolyte periodic addition of water is necessary to maintain the concentration above the top of plates and soon after the addition battery is discharged to lessen the sulfation due to which capacity loss occurs. Self-discharge and ground-shunt hazards are caused due to seepage of acid on the top cover of the battery which leads to a leakage of current [12, 24].

To overcome the aforesaid problems, valve-regulated lead acid (VRLA) batteries based on oxygen-recombination cycle [12-15, 22-23], which is nothing but the oxygen, which generates at the positive plate during charging, combines at the negative plate as shown below have emerged [16-21]. These batteries offer the freedom of battery placement, cyclability without the addition of water or checking the electrolyte specific gravity, increased safety, and superior performance [12-15].

At the positive plate:



At the negative plate:



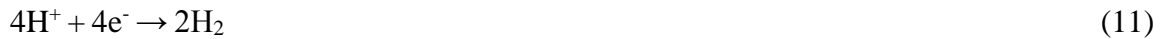


In VRLA cells the electrolyte is completely immobilized in the separator and the active materials, and sufficient void space is left for oxygen to diffuse through the separator to the negative plate and offers completely maintenance free batteries.

Even though VRLA designs are optimized in all directions still these batteries suffer from the following unwanted side reactions.

(a) Hydrogen evolution at the negative electrode and grid corrosion at the positive electrode together cause **water loss** [16-21].

(i) Hydrogen evolution according to



(ii) Grid corrosion according to



In overall:



The water loss must be kept low as low as possible since it gradually increases the concentration of electrolyte and decrease its volume and thus influences the performance of the battery. Water loss cannot be compensated by adding of water. Water is the main cause for slight decrease of capacity that is observed from the very beginning in cycle test of VRLA batteries to keep grid corrosion and hydrogen evolution as low as possible.

(b) **Self-discharge** at the negative electrode according to



This is followed by reaction with H_2SO_4 forms lead sulfate which is the discharged product



In summary, even though lead-acid battery is an oldest type battery, the technology development of lead-acid batteries has been continuing over the years to have best performance and cycle life. From the earliest flooded batteries, different advanced battery configurations such as VRLA designs are now available, which have been adopted in a wide range of applications. Although lead-acid battery designs have been optimized in the past in several different ways, there are still certain new challenges facing lead-acid battery designers, such as grid corrosion at the positive electrode, water loss, self-discharge at the negative plate, sulfation at both the electrodes, poor charge acceptance of positive electrode, larger curing and formation time and more significantly low energy density because of high atomic weight of lead.

References:

1. G. Planté, *C. R. Acad. Sci. Paris*, **50**, 1860, 640.
2. K. Ji et al., *J. of Power Sources*, 2014,**248**, 307-316
3. A. Kirchev et al., *J. of Power Sources*, 2015 ,**279**, 809–824
4. D. Pavlov, T. Rogachev, P. Nikolov, *J. Power Sources*, 2011,**196**, 5155-5167
5. J. Xiang et al., *J. of Power Sources*, 2013,**241**,150-158
6. J. Valenciano et al., *J. of Power Sources*, 2006 ,**158**,851–863
7. T. Funato, K. Takahashi, M. Tsubota, J. Tabuchi, M. Iwata and Y. Tagawa, *GS News Tech. Rep.*, 1993,**52**, 21.
8. M. Saravanan, P. Sennu, M. Ganesan and S. Ambalavanan, *J. Electrochem. Soc.*, 2013, **160**, A70–A76.
9. M. Saravanan, M. Ganesan and S. Ambalavanan, *J. Power Sources*, 2014, **251**, 20–29
10. A.J. Salkind, A.G. Cannone, F.A. Trumbure, in: D. Linden, T.B. Reddy (Eds.), *Lead acid Batteries*, 3rd ed., McGraw-Hill, New York, 2002, p. 23.17 (Chapter 23).
11. P.T. Moseley and D. A. J. Rand, *J. Power Sources*, 2004, **78**, 2.
12. M. Shimpo, H. Nakashima, S. Sasabe, Y. Kasia, Yuasa Jiho, *J. Power Sources*,1990,**68**,46
13. D. Berndt, *J. Power Sources*, 2001, **95**, 2.
14. D. Berndt, *J. Power Sources*, 2001, **100**, 29.
15. D. Berndt, *J. Power Sources*, 2001, **100**, 79
16. P. Ruetschi, *J. Power Sources*, 2004, **127**, 33
17. M. Pourbaix, *Lectures on Electrochemical Corrosion*, Plenum Press, New York, 1973, pp. 65–67.
18. National Research Council, *International Critical Tables*, vol. 3, McGraw Hill Book Co., New York, 1928, p. 279.
19. A.J. Bard, R. Parsons, J. Jordan (Eds.), *Standard Potentials in Aqueous Solution*, Marcel Dekker, New York, 1985.
20. K.R. Bullock, et al., *J. Power Sources*, 1997, **64**, 139–145.
21. K.R. Bullock, D.H. McClelland, *J. Electrochim. Soc.*, 1976, **123**, 327–331; ECS Extended Abstracts 75-1, NJ, 1975, p. 40.
22. B. Hari Prakash B, A. U. Mane, S K Martha, S A Gaffoor, S A Shiva Shankar and A K Shukla, *Electrochem.Solid-State Lett.*,2004, **66**,7A
23. S.S Misra, T.M. Noveske, S.L. Mraz, A. Williamson, *J. Power Sources*, 2001, **95**, 153.

Chapter 2

Nano Structured Reduced Graphene Oxide (RGO) Coated TiO₂ as Negative Electrode Additive for Advanced Lead acid batteries

2.1 Current Status

Lead-acid battery is available in many designs and its performances have been optimized in the past in several ways, but still there are certain challenges facing by lead-acid battery designers, such as grid corrosion at the positive electrode, sulfation at both the electrodes, and poor charge acceptance of positive electrode, larger curing and formation time and more significantly low energy density due to high mass of lead. Sulfation is the main failure mode of the lead-acid battery, as it decreases the amount of usable active materials which limits their cycle life [1-2].

At partial state of charge (PSoC) deep-cycle batteries used in off-grid and unstable grid renewable energy (RE) telecom and inverter, backup systems are heavily cycled, and are often never fully recharged on a regular basis. Solar panels which are not working properly in intermittent weather conditions or in shady areas often faces the PSoC related issues [3]. Due to operating at PSoC can quickly diminish the life of a battery because of heavy sulfation, which results in frequent, costly battery replacements.

The conventional lead-acid batteries also fail when subjected to high rate partial state of charge (HRPSoC) operations e.g. Hybrid electric vehicles (which makes use of regenerative braking). This operating mode is quite challenging as it involves short period of charge-discharge with high current rates. When the regular batteries are operated under HRPSoC mode they suffers from two major issues, namely low charge acceptance and progressive sulfation at negative plates or negative active material (NAM). Therefore, alone NAM is not helpful to persist under HRPSoC

condition so it is necessary to create a novel structures involving NAM and some additive which will decrease sulfation and will increase charge acceptance [4-7].

To overcome the issues of sulfation, poor charge acceptance, low energy density of LAB, lots of research have been carried out to improve the conductivity of active material through carbon based additive materials, modify the lead current collector, electrolyte additives etc.

In the recent years, carbon based additives to the active mass and carbon collectors have been proposed to overcome the issues of sulfation and energy density.

The carbon-based lead foam was used as positive current collector for LAB which was produced by electrodepositing a uniform and dense lead coating on lightweight carbon foam in fluoroborate system under appropriate conditions. The battery had a high discharge capacity and a good cycling stability, which indicated that the carbon-based lead foam could serve as positive current collector

By using pitch-based carbon foam and a punched lead sheet as the negative current collectors demonstrated by Chen et al. [9] showed improved capacity retention under partial-state-of-charge operation in flooded lead acid batteries.

Jang et al. studied graphite foam electrodes pasted with positive active material (PAM) and negative active material (NAM). Indicating that the graphite foam material has much better electric and thermal conductivity [10].

Recently, phenol-formaldehyde resins used in the development of the carbon honeycomb grids coated with lead-2% tin grid for negative electrodes for 2V/2.5Ah LAB demonstrating 191 deep cycles [11].

Carbon honeycomb grids technology employs new carbon/carbon composites with ordered 3D-structure and the electroplated lead\ tin alloy coating instead of classic LAB current collectors. This technology is very useful for automotive applications like car engine cranking applications, electric scooters, low speed electric vehicles, uninterrupted power supply or renewable energy storage [12].

Discrete carbon nanotube (dCNT) of about 0.16% are incorporated as an additive to both the electrodes which would enhance cycle life >60% and charge acceptance boosts of > 200% without impeding manufacturing processes [13].

To overcome different modes of operations like PSoC, HRPSoC addition of different forms of carbon e.g., carbon black[14-16] ,activated carbon[16-18],graphite[17,20], expanded

graphite[17], carbon nanotubes(CNTs), single walled CNTs (SWCNTs),Multi walled CNTs(MWCNTs)[17,20-22], are effective in extending cycle life through sulfation suppression. As because carbon addition to NAM is considered to be the best strategy to create additional new functionalities, as it tunes both the electrical and structural properties of the material .It is well recognized that carbon additives are the most widely used materials in controlling sulfation.

The carbon additives to the active mass of the electrode provides (i) availability of additional nucleation sites, (ii) restriction of PbSO_4 growth, (iii) enhancement of electrical conductivity, (iv) enhancement of capacitance, (v) reduction of hydrogen over potential, (vi) intercalation of hydrogen into graphite structure with an increase in electronic conductivity which will act as a capacitor, and (vii) electro-osmotic pumping of electrolyte ions in presence of graphite [23-24]. Because of high conductivity and high surface area, addition of carbon to the negative active mass increases the contact between active mass and electrolyte, reduces the formation time [25-29].

Addition of graphene also enhances the electroactive surface area of NAM during PSoC applications. PSoC cycle life has significantly improved by more than 140% after addition of 0.2 wt. % graphene and excellent life of about 17,157 cycles has been achieved the average particle size of PbSO_4 crystals on a Pb plate after a PSoC cycle was found to be reduced by around 25% [29]. Influence of graphene and CNT's on the negative electrodes of valve regulated lead-acid batteries during high-rate partial-state-of-charge (HRPSoC) were also studied in literature [29]. X-Ray diffraction pattern was studied after HRPSoC test [29]. It was found that more PbSO_4 crystals were present on the surface of negative electrodes containing 0.25wt. % SWCNT's leading to the accumulation of irreversible big lead sulfate crystals. Whereas only PbO crystals were formed on the negative electrode (Significantly less PbSO_4) containing 0.25wt. % graphene, which stops the reaction of Pb oxidation. Otherwise, premature failure of the cell occurs [30-31]. From the ongoing discussion it is clear that, graphene facilitate the dissolution of big PbSO_4 crystal with less surface coverage and suppressed the sulfation rate, thereby enhances battery performance and cycle life [32].

Besides carbon additives, transition metal oxides (TMOs) such as Ti_2O_3 , Ga_2O_3 , and In_2O_3 [33] etc. are added to the active mass to improve reversibility of the negative electrode. Among these TMO's, the effect of TiO_2 is mostly studied due to its well defined chemical and granulometric

composition, availability and efficacy. Addition of TiO_2 in the NAM provides steric hindrance to the crystals of PbSO_4 in the electrode pores. The active material resistance and hydrogen over potential were negligible for TiO_2 additive based negative electrode. It was found the addition of 2.5 wt. % of TiO_2 in the negative plates showed good cyclic stability about 205,000 cycles under PSoC cycle test. Higher concentration (5%) of TiO_2 in the negative plates did not perform well, due to blocking of some pores with the excess of additive. While less percentage like 0.5wt. % or 1 wt% also didn't work, may be because it was not sufficient to occupy the larger pores. Due to which aggregation of lead sulfate crystal can occur which can lead to degradation of the battery [34-35].

In overall, carbon based grids have been demonstrated as current collectors for anodes and cathodes of LAB. They have much better electric and thermal conductivity, can support charge/discharge currents over 1C charge-discharge rates. Carbon and TiO_2 based additives have been studied in the literature as well. 0.25 wt. % Graphene additive on the negative electrodes of valve regulated lead-acid batteries exhibited superior cycle life under HRPSoC and PSoC test respectively as graphene enhances the electroactive surface area of NAM during cycling. 2.5wt% TiO_2 additive into the NAM blocks the pores in the negative electrode and improves the cycling stability, above 200000 cycles has been achieved under PSoC cycling.

We propose here nano structured reduced graphene oxide (RGO) coated TiO_2 as an additive to the negative active material (NAM) , which would overcome kinetic problems due to the short diffusion length for ionic transport and a relatively high surface area. Here, our goal is to use nanoparticles is to increase the surface area of electrode. So the presence of RGO coated TiO_2 nanocomposite additives will provide interfacial stability (improves the charge efficiency), slows down hard sulfation, high positive active material utilization by occupying pores on the negative plate. This study allow us to identify the elementary processes that takes place on the negative plates during HRPSoC cycling, high rate discharge.

2.2 Experimental

In the light of aforesaid discussion, this work is focused on nanostructured reduced graphene oxide (RGO) coated TiO_2 as a negative electrode additive. The main goal of this additive is to increase the conductivity of lead acid battery by means of RGO and block the pores on the negative plate by means of TiO_2 . This additive helps in reducing the sulfation on the negative plates, which would automatically increase the conductivity of PbSO_4 . Therefore, our focus was to synthesize RGO coated TiO_2 followed by preparing lab scale LAB electrodes. RGO was synthesized in-situ by exfoliating Graphene Oxide (GO). GO was synthesized by Modified Hummer's Method [37]. RGO coated TiO_2 was synthesized by re-exfoliating GO by Hydrothermal synthesis [38]. All the structural and Physical properties of the materials were studied by X-Ray diffraction, Scanning Electron microscopes, Transmission Electron Microscopes, Raman spectroscopy. The electrochemical aspects are studied by electrochemical Galvano static charge-discharge cycling, and Impedance spectroscopy.

2.2.1 Synthesis of Graphene Oxide (GO) by Modified Hummer's Method

Graphene oxide (GO) was synthesized from graphite powder (China steel Chemical Corporation) using modified Hummer's method. In brief, 0.5 g of graphite and 0.5 g of sodium nitrate were mixed together followed by the addition of 23 ml of conc. Sulphuric acid under constant stirring. After 1 h, 3 g of KMnO_4 was added gradually to the above solution while keeping the temperature less than 20°C to prevent overheating and explosion. The mixture was stirred for 1h, after that heated at 35°C for 1h and the resulting solution was diluted by adding 46 ml of Deionized Water (DIW) under vigorous stirring at 95°C under reflux. After cooling diluted with 100ml DIW and stirred for 1h. To ensure the completion of reaction with KMnO_4 , the suspension was further treated with 30% H_2O_2 solution (10 ml). The resulting mixture was washed with 5% HCl and DIW repeatedly, followed by drying at 60°C , grey colored graphene oxide sheets were thus obtained [37].

2.2.2 Synthesis of Reduced Graphene Oxide (RGO) coated TiO₂ by Hydrothermal Method

Hydrothermal method was employed to synthesize Graphene-TiO₂ nanocomposite [38]. 15mg of GO was mixed into a solution of 45 ml deionized water and 15 ml of ethanol under sonication for 1 h to re-exfoliate the GO [37] thoroughly, and 1.5g as-made TiO₂ powder (Sigma Aldrich) was added to the GO suspension. This is followed by sonication and stirring alternately for 2 h. with 30 min for each step until a homogeneous suspension was achieved, which shows a uniform light gray color. The suspension was then poured into a Teflon-lined autoclave of 125 ml capacity and maintained at 120°C for 3 h. to synthesize RGO coated TiO₂ composite. This process simultaneously reduces GO to RGO by electron donation from ethanol and formed Ti-O-C bonding between TiO₂ and RGO. After cooled down to the room temperature, the suspension was filtered several times with deionized water and the product was dried at ambient condition [39]. Finally RGO coated TiO₂ in the ratio of 1: 100 was obtained and TiO₂ will be coated on RGO after Hydrothermal Synthesis as shown in Fig.2.1. Similarly, we have synthesized RGO coated TiO₂ having composition 1: 3 and 1:10.

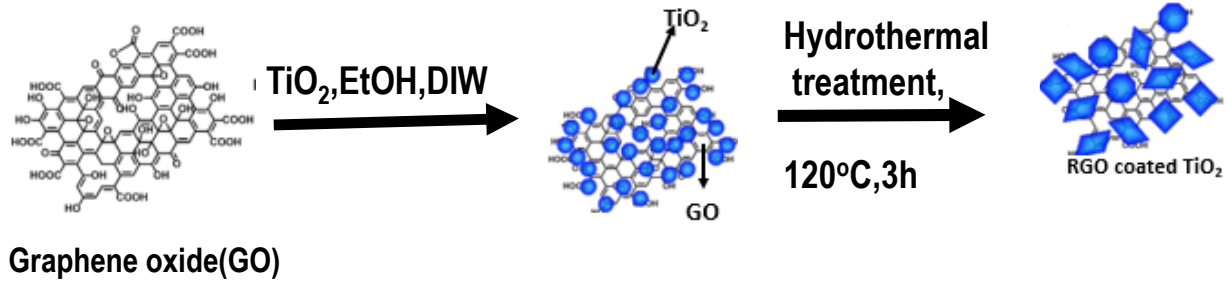


Figure 2.1: Schematic picture of RGO coated TiO₂ after Hydrothermal treatment

2.2.3 Fabrication of Battery Electrodes

Both positive and negative plates are prepared using Pb–Ca–Sn–Al alloy (0.1% of Ca, 1.2% of Sn and 0.03% of Al) grids to construct cells and batteries in Poly(methyl methacrylate) (PMMA) containers using 1.26 specific gravity aq. H₂SO₄ as electrolyte, following an established industrial protocol [40]. In brief, the positive plate paste was prepared by mixing PbO (85 wt. %), sodium carboxy methyl cellulose (0.15 wt. %), Dynel fibres (0.05 wt. %), and aq. H₂SO₄ of 1.4 specific gravity (7 wt. %) with de-ionized water (7.8 wt. %). The negative plate paste was prepared by mixing PbO (85 wt. %), lignin (0.2 wt %), barium sulfate (0.15 wt %), Dynel fibres (0.05 wt %), carbon black (0.1 wt %), and aq.H₂SO₄ of 1.4 specific gravity (7 wt %) with de-ionized water (7.5 wt %), RGO coated TiO₂ (0.5wt. %). The paste densities for positive and negative plates were 4.0 and 4.4gcm⁻³, respectively. After pasting the active materials onto the grids, the plates were subjected to hydrothermal curing. Hydrothermal curing is performed at humidity about 95% at 65°C for about 24 hrs. Subsequently the plates are dried in the curing chamber at 65°C for about 12 h [41].

2.2.4 Cell Assembly

2V/2.1Ah cells were assembled with RGO-TiO₂ added to the negative active mass and using conventional negative electrodes (without additive). The test cell was assembled with 1 negative and 2 positive plates for cell with AGM separator. The cells were filled with 80ml of 1.26 sp. gravity of H₂SO₄. The performance of the cells was limited by the negative plate. Dimensions of the negative and positive plates were (5.5cm X 4.5cm) respectively.

2.2.5 Structural Physical characterizations

The structures were characterized using X-ray diffraction studies (XRD), Scanning electron microscopy (SEM), Transmission electron microscopy (TEM), Raman spectroscopy, four probe conductivity method.

XRD measurements of synthesized GO and RGO coated TiO₂ were performed using PANalytical X'Pert PRO diffractometer (reflection $\theta - \theta$ geometry, Cu K α radiation, receiving slit of 0.2mm scintillation counter, 40mA, 40 kV). The diffraction data were collected at 0.0164 step size, widths over a 2 θ range from 10 to 100. The structural parameters were refined by X'Pert High score Plus software and data is matched with Joint Committee on Powder Diffraction Standards (JCPDS) data.

The morphology of the as-prepared graphene oxide (GO) and RGO coated TiO₂ were estimated by high resolution Field Emission Scanning Electron Microscopy (FE-SEM) using Zeiss supra 40 scanning electron microscope (Carle Zeiss AG, Germany).

The morphology of RGO coated TiO₂ were characterized by high resolution TEM (HR-TEM) (JEOL USA JEM-2100Plus Transmission Electron Microscope).

Synthesized GO and RGO coated TiO₂ were also characterized by Raman spectroscopy using a micro-Raman spectrometer Bruker Senterra using OPUS software.

The electrical conductivity of the RGO coated TiO₂ composite powders were determined by four probe technique. The resistivity values obtained by 4 probe technique were converted to corresponding electrical conductivity or specific conductance (which is reciprocal of electrical resistivity) by using Ohms law. The conductivity was measured by making a cuboid pellet with dimensions of length (1mm), width (2mm) and height (4mm) under a pressure of 2 tons by Hydraulic press.

$$R = \rho \cdot l / A \qquad \sigma = 1 / \rho$$

Where R= Resistance of a sample

l = Length between two conducting points

A = area of the sample

σ = Electrical conductivity

ρ = Resistivity

2.2.6 Electrochemical performance studies

The influence of RGO coated TiO₂ on the cycle life of LABs under high rate discharge conditions were investigated by using 2V/2.1Ah cells. The Galvano static charge-discharge voltage profiles and cyclability data were collected using a programmable battery cycler in the potential ranges between 1.75 V and 2.6 V using constant current.

Cycling studies: The cells were formed using constant current charge-discharge protocol at C/20 rate for 3 cycles till stable capacities are obtained. Subsequently, cycling were performed at low rates i.e. C/10, C/5. After the different C – rate charge-discharge cycling, the cells were subjected to 1C rate cycling using the constant current (CC) protocol, eg.CC charging at 1C till the voltage reaches 2.6V followed by CC charging at C/20 rate till 2.6 V. Subsequently the cells were given 2hrs rest and discharged at C/2 rate (CC discharging) till the voltage reaches to 1.75 V.

Electrochemical impedance studies: Electrochemical impedance spectroscopy (EIS) is a very useful tool to obtain the electrical resistive properties of the electrodes. EIS measurements were carried out in the frequency range between 1 MHz and 10 mHz at an amplitude of 10 mV using Solartron Analytical 1255 FRA (frequency response analyzer) (from Solartron analytical, Oak Rige, TN, USA). Zview software (Scribner Associates, USA) was used to analyze the EIS data. EIS were performed during 15th cycle with the conventional and 0.5 wt. % additive cell at fully charged condition (SoC 1).

2.3 Results and Discussions

2.3.1 X-Ray diffraction

The phase identification of graphite, TiO₂, GO, RGO and RGO coated TiO₂ were determined by XRD. The XRD results for graphite, GO and RGO are shown in Figure 2.2 (a) and RGO, TiO₂, and RGO coated TiO₂ are shown in Fig. 2.2 (b) respectively. The XRD pattern of graphite showed a peak at 26° corresponding to the plane (002). For GO, a small change in the position of the principal reflection is observed at $2\theta=10.5^\circ$ having interlayer spacing about 9Å. This is due to the oxidation of double bonds containing functional groups (epoxy groups, carboxylic groups) attached on both sides of the graphene sheets (Fig. 2.2 (a)).

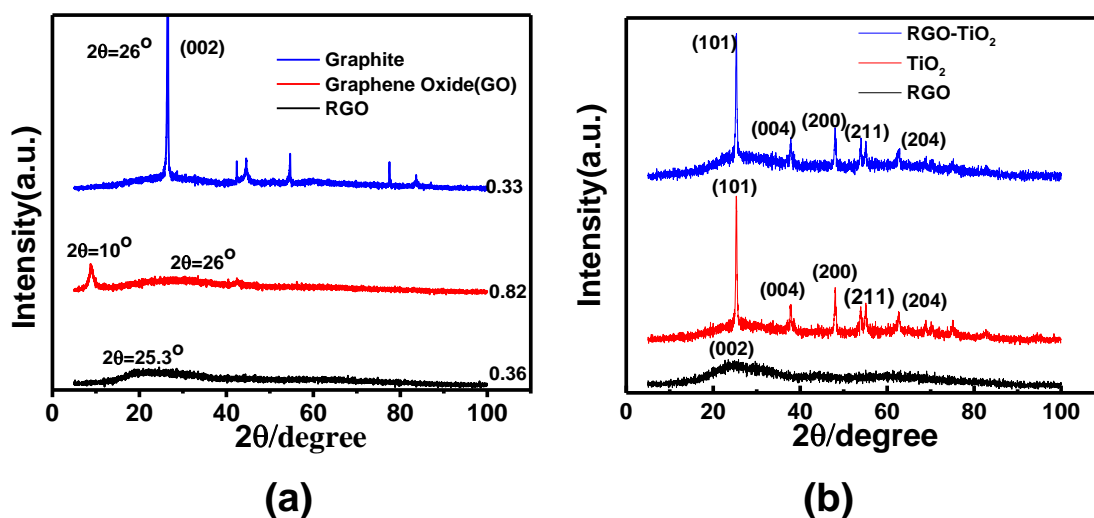


Figure 2.2 (a) Powder XRD patterns of Graphite, Graphene Oxide, RGO and (b): Powder XRD patterns of RGO-TiO₂, TiO₂, and RGO

XRD patterns in Fig. 2.2 (b) shows RGO nano sheets have a weak (002) diffraction line; indicating that RGO layers are separated by TiO₂ nanoparticles, form a detectable graphite structure. This indicates that RGO is comprised mainly of single layer sheets. The (101) peak for composite is much broader than TiO₂. This peak broadening suggest the interaction of TiO₂ with RGO and also distortion of lattice structure of TiO₂ [32].

2.3.2 Morphology of GO and RGO-TiO₂ composite

The morphology in Fig. 2.3(a) shows the layered structure of graphite in which many graphene layers (thickness of each graphene layer is ~ 10s of nm) are stacked together. The morphology of GO is presented in Fig.2.3(b) shows the multi-layer structure with a greater distance between layers ($d=0.82\text{nm}$) indicating the presence of oxygen containing functional groups like epoxy, alcohols, carboxylic acids, quinone groups as compared to graphite having less between the layers($d=0.34\text{nm}$). SEM in Fig.2.3 (c) shows that reduced graphene layers are stacked together with a distance between the layers (0.36nm) as oxygen functionalities are removed. SEM in Fig.2.3(c) shows spherical morphology of TiO₂ particles having sizes are in the range of 25-50nm. Nanocrystalline nature of RGO coated TiO₂ is confirmed in the Fig.2.3 (d). RGO coated TiO₂ has also spherical morphology similar to pristine TiO₂ as the concentration of graphene to TiO₂ are in the ratio of 1: 100.

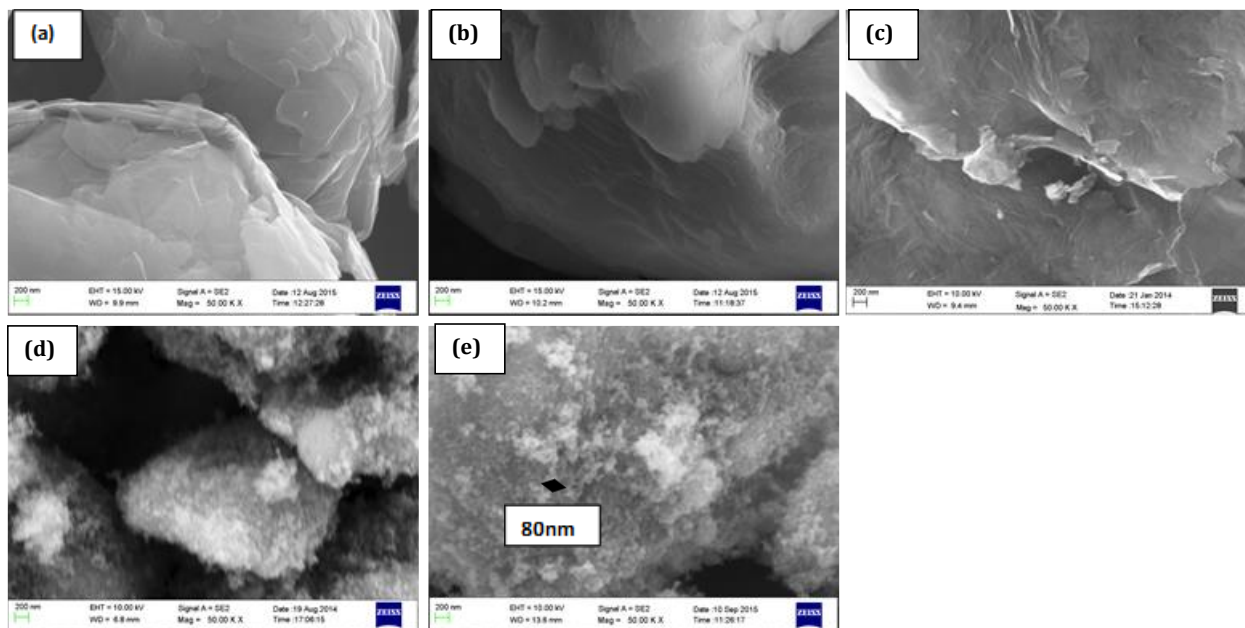


Figure 2.3: SEM pictures of (a) Graphite, (b) Graphene Oxide, (c) RGO, (d) TiO_2 - anatase, (e) RGO coated TiO_2

2.3.3 Morphology of RGO coated TiO_2 (1:10) by Transmission electron microscopy

The morphology of RGO coated TiO_2 (1:10) was further characterized by high resolution TEM (HR-TEM) (JEOL USA JEM-2100Plus Transmission Electron Microscope). From the Fig.2.4 it is very clear that 5-10 nm's of RGO is coated clearly onto TiO_2 nano-particles. The size of RGO coated TiO_2 particles are in the range of 20-40 nm.

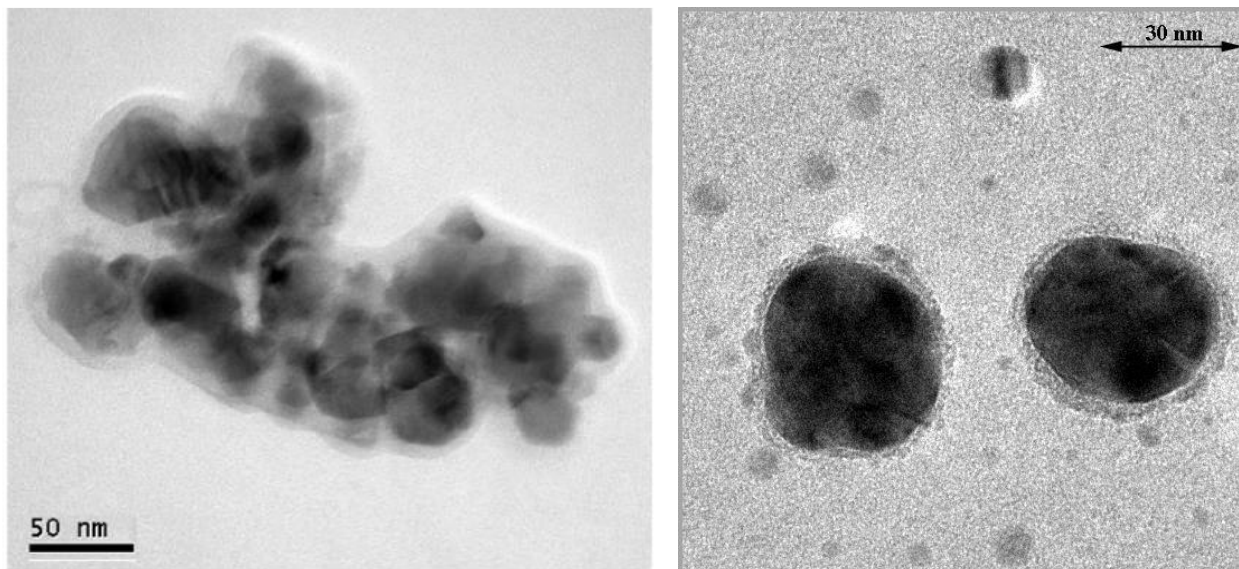
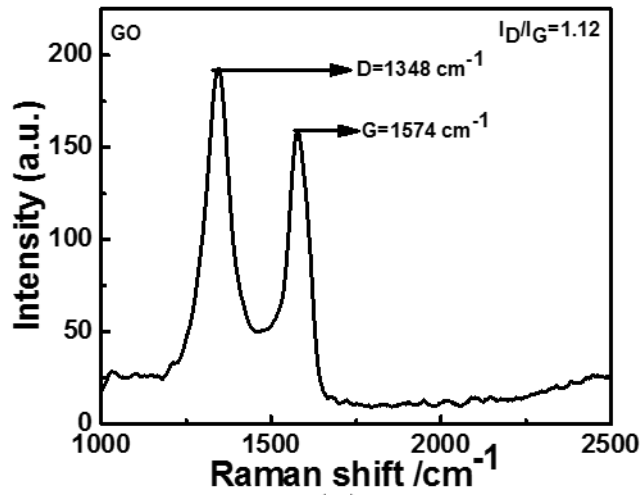


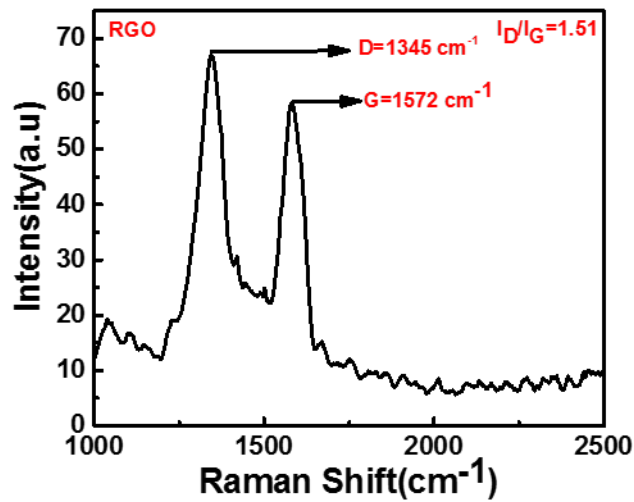
Figure 2.4: TEM pictures of RGO coated TiO₂ (1:10)

2.3.4 Characterization by Raman Spectroscopy

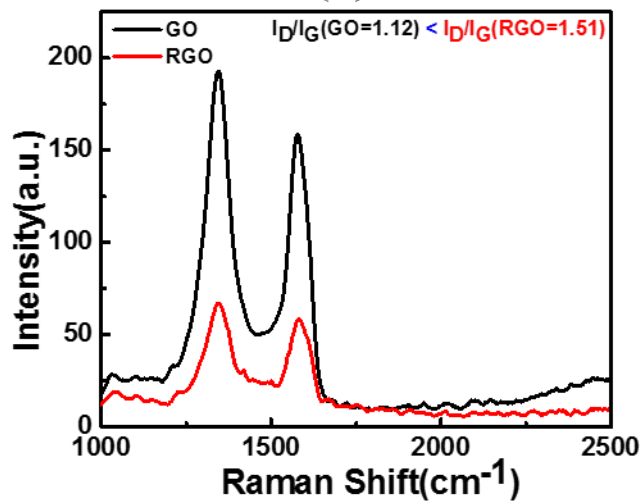
Raman spectroscopy has been accepted to be a versatile and purely optical technique for the characterization of graphene based materials. The reduction process of GO can manifest itself in Raman spectra by the changes in the relative intensity of two main peaks: D and G. This information verify the reduction processes. The D peak of GO located at 1348 cm^{-1} as shown Fig.2.5 (a) and 1346 cm^{-1} for RGO as shown in Fig.2.5 (b). The other one is the G band (Graphitic band) of GO at 1574 cm^{-1} as shown in Fig.2.5 (a) and 1572 cm^{-1} for RGO as shown in Fig.2.5 (b) corresponds to sp^2 bonded carbon atoms, slightly down shifts. This allows definite, high throughput, nondestructive identification of graphene layers. From the Fig.2.5(c), intensity ratio for reduced graphene oxide i.e. I_D/I_G is 1.51 nearly 1 and $\frac{1}{2}$ times as comparison to that GO whose I_D/I_G ratio is 1.12. This means that more sp^2 bonds are present in RGO. This happens due to the significance increase in size of the in-plane sp^2 domains due to removal of oxidative functional groups on re-exfoliation which clearly indicates almost double the conductivity of RGO compared to GO.



(a)



(b)



(c)

Figure 2.5: Raman spectra of (a) GO, (b) RGO and (c) GO and RGO

Raman studies of RGO-TiO₂ {001} Nano composite:

Raman spectra of RGO-TiO₂ is presented in Fig.2.5 (d), a very intense peak is observed at E_g (143.4 cm⁻¹) for Ti-O which matches with the literature value. D and G bands are also observed having very less intensity and they are broadened due to the presence of isolated double bonds separated by functional groups on the carbon network of GO. The Raman spectrum of RGO coated TiO₂ shows peaks in the low frequency region pertaining to the B_{1g} (400 cm⁻¹), A_{1g} (513 cm⁻¹) and E_g (637 cm⁻¹) modes of the anatase phase as shown in Fig.2.5 (d). The intensity of the D band (1348cm⁻¹) is found to be decreased compared to that of RGO, and the wavenumber is shifted slightly lower, indicating the formation of the RGO coated TiO₂ nanocomposite. The intensity ratio of D/G of RGO coated TiO₂ is found to be low (0.87) compared to that of RGO (1.51), due to the increased average size of the sp² domain due to the removal of oxygen functionalities and defects in RGO. In case of the GO sheet, a decreased D/G intensity ratio is observed, suggesting that the defects in the reduced graphene oxide increase after the reduction of GO.

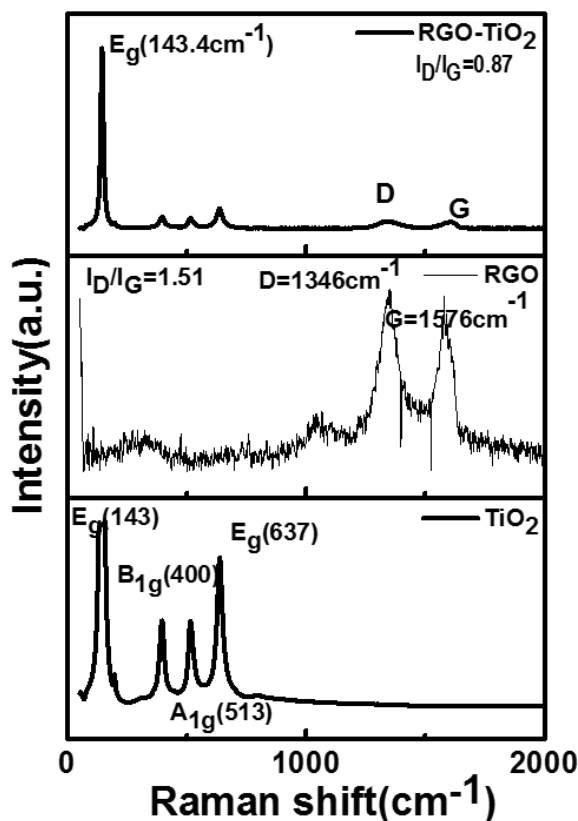


Figure 2.5 (d): Raman spectra of TiO₂, RGO and RGO coated TiO₂

2.3.5 Four Probe Conductivity Measurement

The resistance of the RGO-TiO₂ composite was evaluated by 4 probe conductivity measurement and data is presented in Fig. 2.6. The slope in the Fig.2.6 shows the resistance of 4.85kΩ which is very high, so conductance is very low (0.025 S/m). The conductance is low due to less weight percentage of GO (1% of GO and 100% of TiO₂). The conductivity of the composite is improved with increase in compositions of RGO and the data is not analyzed yet.

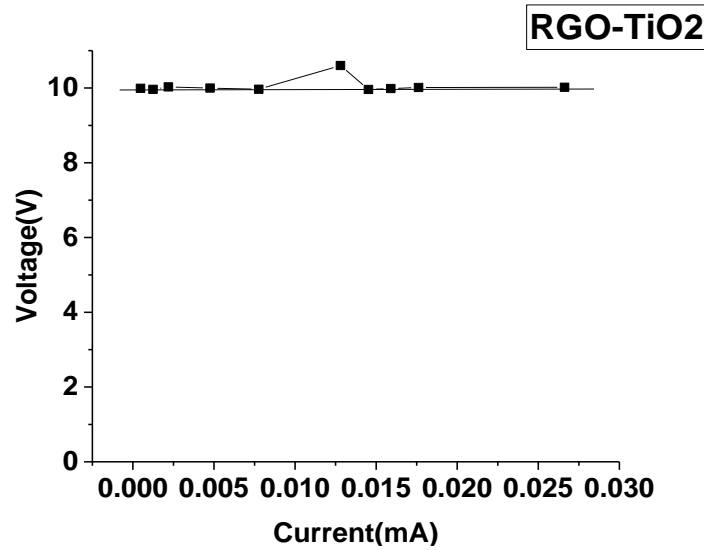


Figure 2.6 Electrical conductivity by four probe technique

(The Electrical conductivity, $\sigma = L/R*w*h = 1\text{mm}/4.85\text{k}\Omega *2\text{mm}*4\text{mm} =0.025 \text{ S/m}$)

2.3.6 Electrochemical characterizations

The influence of nano-structured RGO coated TiO₂ on the advanced LAB are studied with different weight percentages (1:100, and 1:10 wt. % of 0.25wt. %, 0.5wt. %, 1wt. %RGO to TiO₂) on to negative active mass. Initially, negative electrodes were prepared using 0.25 wt% RGO coated TiO₂ (RGO: TiO₂ was 1: 100) in the NAM. The cycling data at different C rates for 0.25 wt. % RGO coated TiO₂ and conventional 2.1 Ah lead-acid cells are presented in Fig. 2.7. A very small increment ($\approx 5\%$) in capacity was observed for the 0.25 wt. % RGO coated TiO₂ electrodes compared to the conventional LAC at all C rates between C/20 and 2C rate. This could

be due to less weight percentage of additive (0.25 wt. % RGO coated TiO₂) in the negative active material and less percentage of GO (1% compared to TiO₂ 100%).

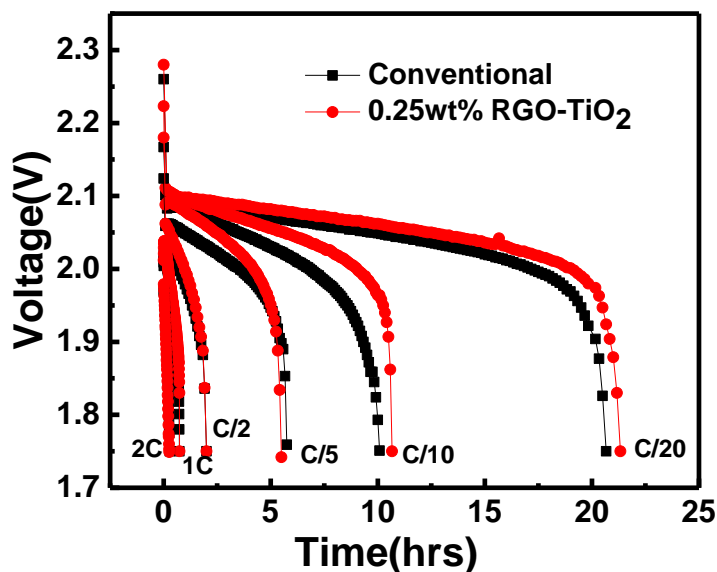


Figure 2.7: C-Rate Discharge curves of 0.25wt% RGO coated TiO₂

The weight percentage was further optimized by taking the literature composition of TiO₂ i.e. 2.5wt% of TiO₂ gives good cycling stability up to 20,000 HRPSoC cycles [26]. So various composition of RGO to TiO₂ such as 1:10 (in which GO is 0.25wt% and TiO₂ is 2.5wt%) and 1:3 wt. % of RGO to TiO₂ (in which GO is 0.25wt% and TiO₂ is 0.75wt%) were prepared and used as an additive (0.5 % optimized) for negative electrodes for the lead-acid cells. The electrochemical performances at different C rates were evaluated in 2.1 Ah lead-cells. Very good electrochemical performance of the cells were achieved with 0.5 wt. % RGO coated TiO₂, additive based negative active material. The charge discharge voltage profiles for the first formation cycle is shown in Fig. 2.8 (a) and (b). The charge profiles in Fig. 2.8 (a) clearly indicates that more charge acceptance, less hydrogen evolution for the 0.5 wt.% RGO coated TiO₂, additive based cells compared to conventional cells. In conventional LAC, during charge conversion of lead sulphate back to lead (Pb) is difficult. But the additive cell accepts more charge due to the presence of RGO which acts as a charge storing capacitor and helps in the conversion of Pb²⁺ → Pb. During the first formation cycle an increase in capacity of about >55% at C/20 rate is achieved for 0.5 wt. % RGO coated

TiO₂ additive based cells compared to the conventional LAC (Fig.2.8 (b)). The RGO coated TiO₂ additive based cells are formed in the 1st cycle whereas conventional electrode takes about 3 cycles to achieve the full capacity. Beside the voltage of the RGO coated TiO₂ additive based cells are about 0.1 V higher than that of conventional cells indicating lesser electrode resistance, less surface film formation (PbSO₄) and delivering higher capacity.

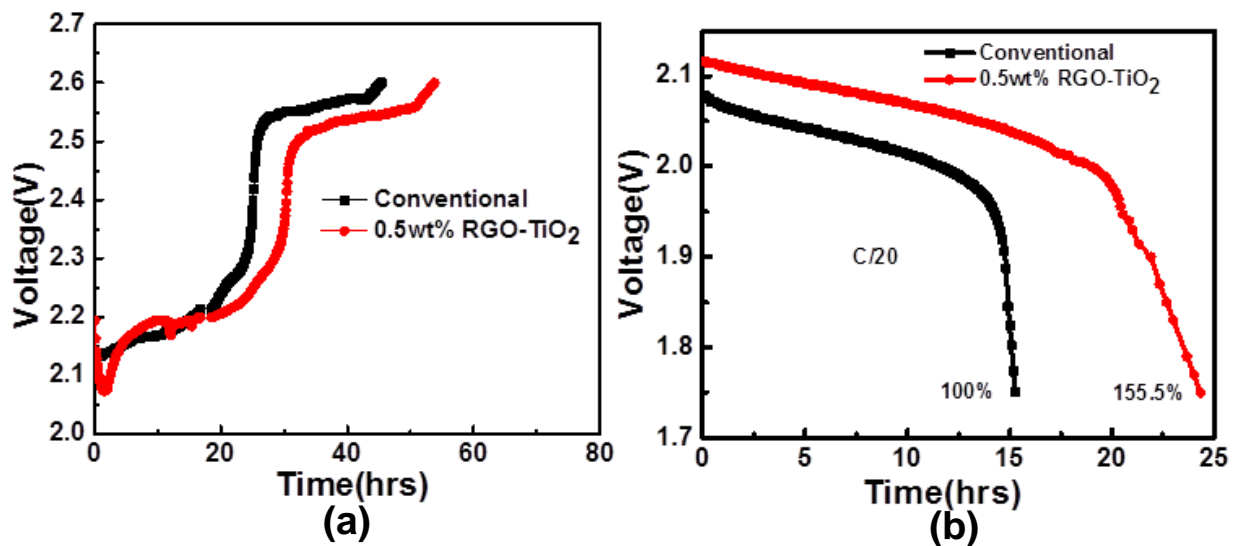


Figure 2.8 (a) Charge curve of 0.5wt% RGO coated TiO₂ (b) Discharge curve of 0.5wt% RGO coated TiO₂ at C/20 rate at 25 °C.

After 3 formation cycles, the cells were charge-discharged at different C rates from C/20, C/10, C/5 as shown in Fig. 2.9. 0.5wt% RGO coated TiO₂ based LAC has higher plateau voltage at all C rates compared to conventional, indicating less electrode impedance values, and thus these electrodes deliver an increase in capacity of about 20% at low discharge rates of C/20-C/5. These results indicate the RGO coated TiO₂ shows improved rate capability. Moreover, the discharge capacities indicate the contact resistance between the NAM/grid has a strong effect on the electrochemical performance. The impact was observed in the charge acceptance of a battery and was attributed to the RGO in negative active mass.

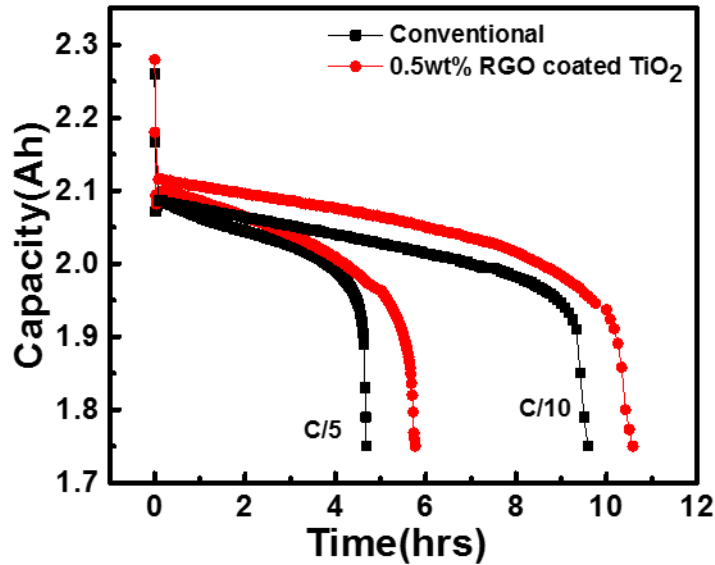


Figure 2.9: C-rates (C/10 and C/5) discharge curves of 0.5wt% RGO coated TiO₂ additive cell and conventional cell

Charge and Discharge performance at 1C rate:

Beside C/20-C/5 charge discharge rate performances, cycling experiments were also conducted at high C rates (1C). The data in Fig. 2.10 (a-b) shows that less electrode impedance (less charge voltage and high discharge voltage plateau) at 1C rate. Beside the charge profile clearly indicates less H₂ evolution and more charge acceptance due to the presence of RGO for the additive based cell compared to conventional cells. Higher discharge capacity of about 40% was achieved for the additive based cell compared to conventional cell indicating the suitability of this electrode for high rate discharge applications such as HEV's and EVs.

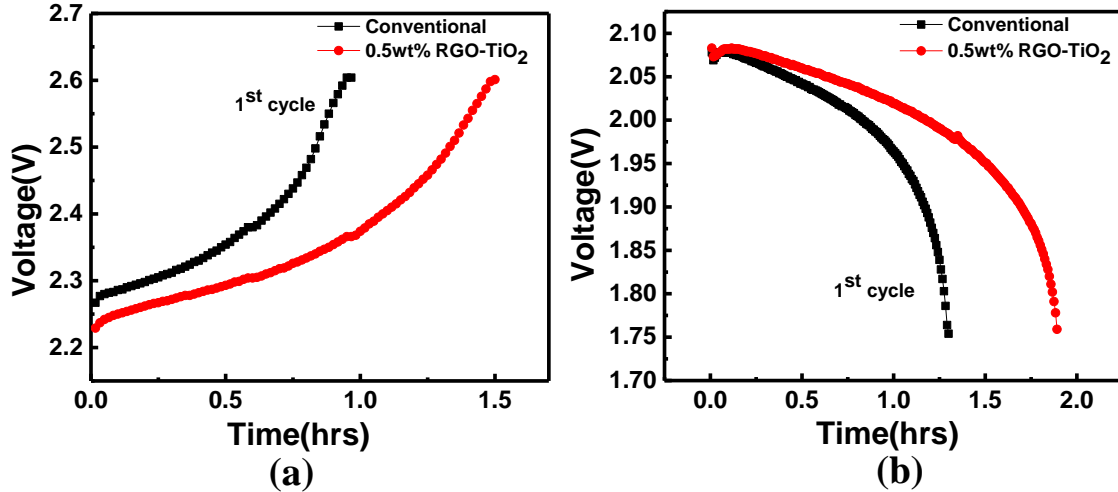


Fig. 2.10 (a) Charge voltage profile 0.5wt% RGO coated TiO₂ at 1C rate (b) Discharge voltage profile of 0.5wt% RGO coated TiO₂ at 1C rate

Cycle life study at 1C:

Cycling study (Fig.2.11) was performed on 2V/2.1Ah conventional and 0.5 wt. % RGO coated TiO₂ additive experimental cell at 1C rate. An increase in capacity of about 40% was observed with RGO coated TiO₂ additive based cells as compared to conventional cells. This could be due to the reversibility of PbSO₄ to lead. As cycling progresses, conventional cell has poor capacity retention due to the formation of hard PbSO₄ at the negative plate. While in case of additive based cell, grid and negative active material layer contributes to high charge transfer and transfer the electrons for the conversion of Pb²⁺ → Pb due to presence of RGO. RGO makes a good electronic contact along the active particles, and on the current collector thereby providing high electronic conductivity and better electrochemical performance at high C rates. Besides addition of RGO coated TiO₂ in NAM could limit the sulfation of negative plates, due to the high porosity of graphene which could acts as an electrolyte reservoirs in the interior of the negative plates. This helps the active sites for the migration of PbSO₄ to Pb during charge and inhibition of PbSO₄ during cycling. The obtained results indicates that more active material utilization of negative active mass during 1C rate cycling for the additive based cell. Formation of tetra basic lead sulfate is more significant in the presence of TiO₂ which enhances the cycle life of the lead acid battery. These results shows the presence of RGO coated TiO₂ in negative active material has the ability to accept large charging currents and limit the growth of PbSO₄ crystal thereby delivering high

capacity. This is clear that nano-structured RGO coated TiO_2 is suitable for high rate discharge (1C rate) and initial capacity of 1.9Ah capacity could be obtained (>40% Capacity) and stable over 50 cycles. The decay in capacity is due to deep discharge and high voltage cycling up to 2.6V. One can expect high H_2 evolution and active material degradation during such harsh cycling's.

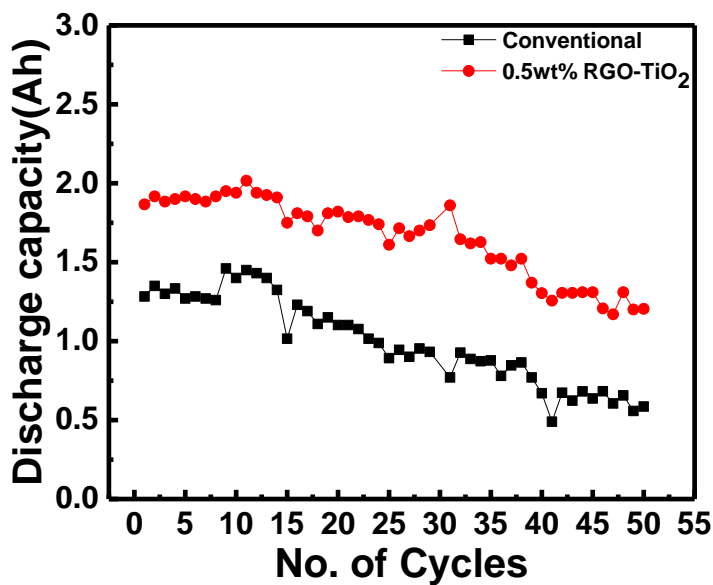


Figure 2.11: Cyclic stability of 0.5wt% RGO coated TiO_2 (1:10) at 1C rate.

2.3.7 Electrochemical Impedance Studies

The impedance plots of 0.5 wt. % RGO coated TiO₂ additive and conventional cells are shown in Fig.2.12. Impedance is taken after 15th cycle of charging and here we get less ohmic resistance, R_Ω (includes the resistance of electrolyte, current collectors, battery terminals, and inter-cell connectors), less surface layer resistance, R_{surface} (resistance due to formation of lead sulphate layer on negative plates during discharging) and less charge transfer resistance, R_{CT} (electron transfer from electrode to electrolyte and vice-versa) for the additive 0.5wt. % of RGO coated TiO₂ as compared to conventional as shown in Table 1. Therefore, total resistance for the additive cell is much lesser compared to conventional LAC.

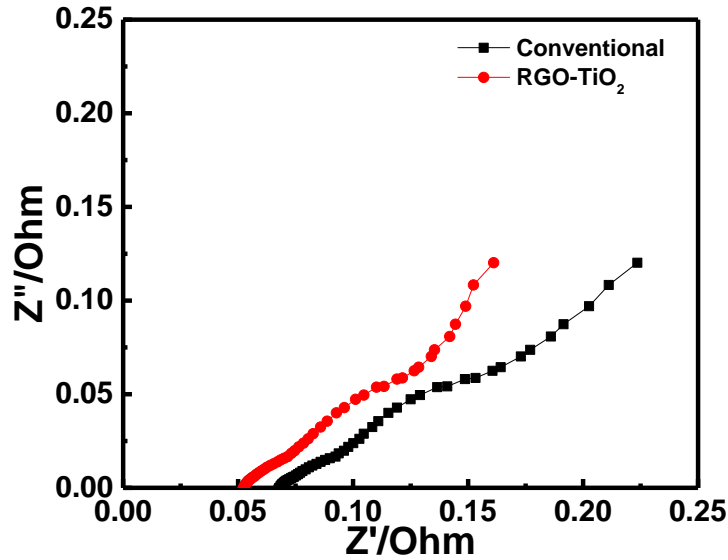


Figure 2.12 EIS after 15th cycle of charging for 0.5 wt. % RGO coated TiO₂ additive and conventional cells

| | Conventional | 0.5wt. % RGO coated TiO ₂ (1:10) |
|----------------------|--------------|---------------------------------------------|
| R _Ω | 0.07Ω | 0.05Ω |
| R _{Surface} | 0.12Ω | 0.09Ω |
| R _{CT} | 0.23Ω | 0.175Ω |
| R _{total} | 0.42Ω | 0.31Ω |

Table 1. Resistance values for 0.5 wt. % RGO coated TiO₂ additive and conventional cells.

2.3.8 Tear-down analysis

Tear down analysis was performed after the completion of 50 charge-discharge cycles at 1C rate. In this experiment, NAM was extracted from the grid, washed thoroughly in de-ionized water, subjected to drying at 60°C for 48hrs. After drying, XRD of the NAM was performed. It was found that conventional LAC consists of more lead sulfate crystals (Fig.2.13 (a)) as compared to additive 0.5wt. % RGO coated TiO₂ (1:10) NAM. In case of additive 0.5wt. % RGO coated TiO₂ more crystals of 4-BS (4PbO.PbSO₄) are observed which indicates that during formation cycles all active material is not completely converted into lead and some crystals of 4-BS are left which built 3D network structure on the grid which provides a mechanical support to NAM, preventing it from the shedding and conducts the current at every point throughout the plate as shown in Fig. 2.13 (b). Therefore, presence of 4-BS gives good cycling life and this happens due to the presence of TiO₂.

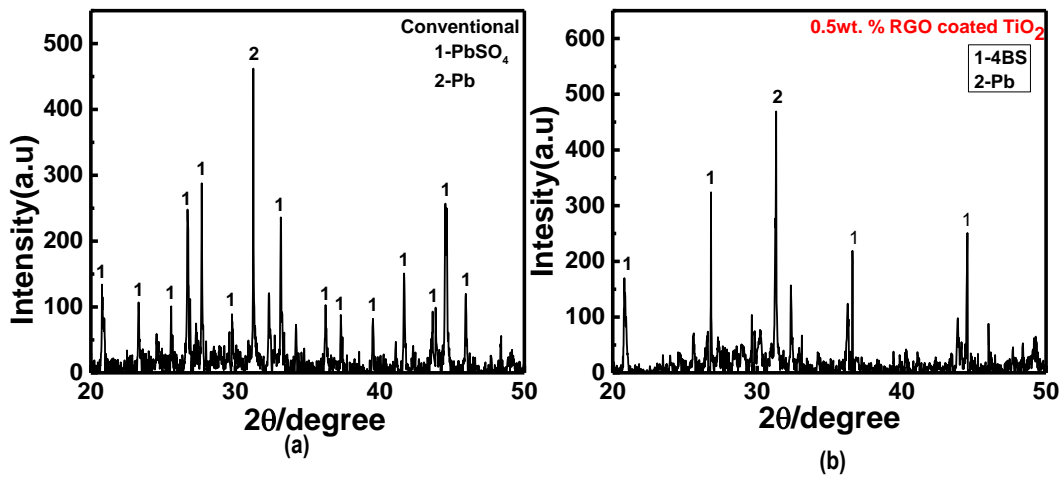


Figure 2.13 XRD pattern (a) Conventional negative active material, (b) 0.5wt. % RGO coated TiO₂ (1:10) additive negative active material

2.3.9 On- going work

The influence of RGO coated TiO₂ on electrochemical performance of LAB are also studied by increasing the composition of RGO: TiO₂ from 1:10 to 1:3 (0.25wt. % of GO and 0.75wt. % of TiO₂). Negative electrodes were prepared using 0.25 wt. %, 0.5wt. %, 1wt. % of RGO coated TiO₂. But results of 0.5 wt. % of RGO coated TiO₂ found to give better electrochemical performance. 0.5 wt. % of RGO coated TiO₂ (1:3) to the NAM delivers excellent capacity >95% compared to conventional cell during the 1st cycle, reduces formation cycle to 1 cycle which significantly reduces production cost. The discharge performance data during 1st cycle for the 0.5 wt. % of RGO coated TiO₂ (1:3) to the negative active mass and conventional lead-acid cell are shown in Fig.2.14. Further studies such as C rate performance, cycle life studies, EIS, HRPSoC and tear-down analyses are under progress.

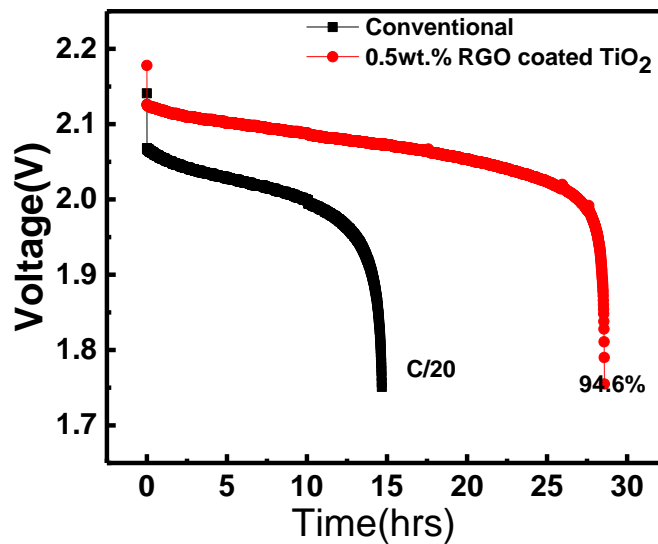


Figure 2.14 Discharge voltage profile of 0.5wt. % RGO coated TiO₂ (1:3)

Conclusion

GO was synthesized by modified Hummers method. RGO coated TiO_2 was synthesized by hydrothermal synthesis. Addition of 0.5 wt. % of RGO coated TiO_2 to the negative active mass in which composition of RGO: TiO_2 is 1:10 delivers > 55% capacity during the first formation cycle. 0.5 wt. % of RGO coated TiO_2 (1:10) to the negative active mass increases the battery formation efficiency from 3 cycles to 1 cycle as compared to conventional LAC. 0.5 wt. % of RGO coated TiO_2 (1:10) to the negative active mass provides good charge acceptance due to the presence of RGO indicating reversibility of lead sulfate which reduces progressive sulfation on negative electrode. TiO_2 helps increase cyclability. 0.5 wt. % of RGO coated TiO_2 (1:10) to the negative active mass delivers > 40% increment in capacity at 1C rate for 50 cycles as compared to conventional LAC. Addition of only 0.5 wt. % RGO coated TiO_2 additive to the NAM may help to operate the cells high rate discharge like HEV's. Tear-down analysis proved the presence of 4-BS crystals in the XRD pattern due to RGO coated TiO_2 additive to the active mass which delivers good cycling life due to the presence of TiO_2 in comparison to conventional cell where more lead sulfate crystals are present. Beside the study was extended to 0.5 wt. % of RGO coated TiO_2 (1:3) to the NAM which delivers again excellent capacity >90% compared to conventional cell during the 1st cycle, reduces formation cycle to 1 cycle. Further studies such as C rate performance, cycle life studies, EIS, HRPSoC and tear-down analyses are under progress.

References

1. R. H. Newnham and W. G. A. Balasing, *J. Power Sources*, 1997, **66**, 27.
2. P. Whitehira, *J. Power Sources*, 1993, **42**, **195**.
3. J. Liu, *Adv. Funct. Mater.*, 2013, **23**, 924–928
4. P. T. Moseley, *J. Power Sources*, 2009, **191**, 134-138
5. D. Pavlov and P. Nikolov, *J. Power Sources*, 2013, **242**, 380.
6. K. Nakamura, M. Shiomi, K. Takahashi and M. Tsubota, *J. Power Sources*, 1996, **59**, 153.
7. M. Shiomi, T. Funato, K. Nakamura, K. Takahashi and M. Tsubota, *J. Power Sources*, 1997, **64**, 147
8. K. Ji et al., *J. Power Sources*, 2014, **248**, 307-316
9. *Electrochimica Acta*, 53, Issue 5, 1 January 2008, Pages 2245-2249
10. *J. Power Sources*, **161**, Issue 2, 27 October 2006, Pages 1392-1399
11. A. Kirchev et al., *J. Power Sources*, 2011, **196**, 8773–8788
12. A. Kirchev et al., *J. Power Sources*, 2015, **279**, 809–824
13. N. Sugumaran et al., *J. Power Sources*, 2015, **279**, 281-293
14. D. Pavlov, T. Rogachev, P. Nikolov and G. Petkova, *J. Power Sources*, 2009, **191**, 58-75
15. D.P. Boden, D.V. Loosemore, M. A. Spence and T.D. Wojcinski, *J. Power Sources*, 2010, **195**, 4470-4493
16. P. Krivák et al., *J. Power Sources*, 2012, **209**, 15–19
17. S. Logeshkumar and R. Manoharan, *Electrochim Acta*, 2014, **144**, 147-153
18. J. Xiang et al., *J. Power Sources*, 2013, **241**, 150-158
19. M. Fernandez, J. Valenciano, F. Trinidad and N. Munoz, *J. Power Sources*, 2010, **195**, 4458-4469
20. P. Tong, R. Zhao, R. Zhang, F. Yi, G. Shi, A. Li and H. Chen, *J. Power Sources*, 2015, **286**, 91-102
21. K. Micka, M. Calabek, P. Baca, P. Krivák, R. Labus and R. Bilko, *J. Power Sources*, 2009, **191**, 154-158
22. R. Shapira, G. D. Nessim, T. Zimrin and D. Aurbach, *Energy Environ. Sci.*, 2013, **6**, 587-594
23. K. Nakamura, M. Shiomi, K. Takahashi, M. Tsubota, *J. Power Sources*, 1996, **59**, 153

24. M. Shiomi, T. Funato, K. Nakamura, K. Takahashi, M. Tsubota, *J. Power Sources*, 1997, **64**,147
25. M. Saravanan, M. Ganesan and S. Ambalavanan, *J. Power Sources*, 2014, **251**, 20-29
26. D. Pavlov, P. Nikolov and T. Rogachev, *J. Power Sources*, 2011, **196**, 5155-5167
27. B. Hong, L. Jiang, H. Xue, F. Liu, J. Li and Y. Liu, *RSC Adv.*, 2014, **4**,33574-33577
28. M. Saravanan, P. Sennu, M. Ganesan and S. Ambalavanan, *J. Electrochem. Soc.*, 2013, **160**, A70-A76
29. D. Pavlov and P. Nikolov, *J. Power Sources*, 2013, **242**, 380-399
30. *RSC Adv.*, 2015, **5**, 71314–71321
31. S. M. Kumar, S. Ambalavanan and S. Mayavan , *RSC Adv.*, 2014, **4**, 36517-36521
32. L. Zhao et al., *J. Power Sources*, 2014, **248**,1-5
33. *Int. J. Electrochem. Sci.*,2016,**11**
34. M. Cal´abek et al., *J. Power Sources*, 2006, **158**,864–867
35. K. Micka et al.,*J. Power Sources*, 2009, **191**,154–158
36. L. Shahriary, **Vol. 02**, No. 01, January 2014
37. Materials and processes for energy: communicating current research and technological developments (A. Méndez-Vilas, Ed.)
38. D. Pavlov, Lead acid Battery Book, 2011, P.No.311-361
39. D. Pavlov, Lead Acid Battery Book, 2011, 443-479
40. *J. Mater. Chem.*, 2011, **21**, 3415–3421